minerals

Article

Tectono-Magmatic Significance of the Lower Devonian Mafic Intrusions in the East Kunlun Orogenic Belt: Keys for the Evolution of Proto-Tethys

Yong Meng [1,*], Xin Zhang [1,*], Zuochen Li [2], Yuan Han [1], Haibo Zhao [1], Yang Yang [1] and Xingchen Xu [1]

1 Xining Center of Natural Resource Comprehensive Survey, CGS, Xining 810021, China
2 School of Earth Science and Resources, Chang'an University, Xi'an 710054, China
* Correspondence: myong@mail.cgs.gov.cn (Y.M.); gallary_zx@163.com (X.Z.)

Abstract: Studies on post-collisional magmatic rocks can provide key clues to researching the crust–mantle interactions and the tectonic evolution of collisional orogenic belts. This study investigated a suite of newly discovered mafic intrusions in the middle of the East Kunlun orogenic belt through integrated analysis of petrology, petrography, and zircon U–Pb dating. The data could offer new insights into the generation of the Proto-Tethyan tectonic evolution. The result shows that these mafic intrusions are mainly gabbro and diabase, formed in the Early Devonian, with zircon U–Pb ages of 408.9 ± 2.0 Ma for gabbro and 411.1 ± 3.1 Ma for diabase. It consists of plagioclase, pyroxene, and dark minerals, and a small number of calcite and chlorite. Diabase has a small amount of amygdale. Their $Na_2O + K_2O$ contents range from 3.47 wt.% to 5.45 wt.%, with Na_2O/K_2O ratios from 1.39 to 3.09, suggesting that they are calc–alkaline rocks. These rocks have an $Fe_2O_3{}^T$ content of 7.68 wt.%–11.59 wt.% and $Mg^{\#}$ of 50.58–59.48, belonging to the iron-rich and magnesium-poor type. The chondrite-normalized rare earth elements show similar patterns that are characterized by enrichment of light rare earth elements, with $(La/Yb)_N$ of 3.27–6.75 and no significant europium anomaly, indicating the rocks are homogenous. The studied rocks are characterized by low contents of compatible elements Cr and Ni, enrichment of large-ion lithophile elements such as Rb, U, Sr, and Nd, and high-field-strength elements such as Nb, Ta, Zr, Hf, and Th. The mafic magma originated from the partial melting of the enriched mantle and was assimilated and mixed with crust materials during the process of migration. Based on the regional tectonic evolution, we interpret that the Proto-Tethys Ocean had closed in the Early Devonian, and that the East Kunlun region was in a post-collisional extensional tectonic setting.

Keywords: gabbro; diabase; geochemistry; Early Devonian; East Kunlun orogenic belt; Proto-Tethys

Citation: Meng, Y.; Zhang, X.; Li, Z.; Han, Y.; Zhao, H.; Yang, Y.; Xu, X. Tectono-Magmatic Significance of the Lower Devonian Mafic Intrusions in the East Kunlun Orogenic Belt: Keys for the Evolution of Proto-Tethys. *Minerals* **2023**, *13*, 478. https://doi.org/10.3390/min13040478

Academic Editor: Georgia Pe-Piper

Received: 4 February 2023
Revised: 22 March 2023
Accepted: 23 March 2023
Published: 28 March 2023

1. Introduction

The East Kunlun orogenic belt (EKOB), located in the northeastern part of the Tibetan Plateau, is an important part of the Central orogenic belt (Figure 1a). It is typically characterized by the development of two major tectonic–magmatic cycles associated with the evolution of the Proto-Tethys and Paleo-Tethys. It is also an important site for the study of the tectonic evolution of the Proto-Tethys and Paleo-Tethys in the East Tethys tectonic domain [1–6]. The East Kunlun orogenic belt underwent two major magmatic periods, namely the Caledonian and the Hercynian–Indosinian, forming significant tectonic–magmatic belts and witnessing the tectonic evolution of the Proto-Tethys and Paleo-Tethys [7–19]. Mo et al. [20] developed a tectonic–magmatic framework for the Caledonian motion in the East Kunlun, which divided the Caledonian orogenic cycle in the EKOB into four phases, namely, the ocean basin opening and expansion phase (579–518 Ma), the subduction phase (508–450 Ma), the collisional and post-collisional phase (413–380 Ma), and the post-orogenic collapse and uplift phase. The Proto-Tethys was formed during the opening and expansion phase in the Early Cambrian [4–6,10,21–30], and the subduction and reduction of the Proto-Tethys in the East Kunlun region was mostly confined to the late Early Cambrian–Early Silurian [31–38]. Previous studies have provided lots of information on the opening, spreading, and subsidence of the ocean basin of the Proto-Tethys in the East Kunlun region, but the understanding of its final closure and collisional and post-collisional events are quite limited due to the lack of geochronology and geochemistry evidence. Previously, most scholars considered the final closure and collisional events to have occurred in the Late Silurian–Middle Devonian based on the identification of A-type granites in this region [39,40]. However, a few mafic intrusions of this period have recently been found, including the Early Devonian Lichotag mafic intrusions we discovered in the EKOB. By conducting geochronological and geochemical studies on the Lichotag mafic intrusions, we can provide important information on the tectonic–magmatic evolution during the Late Caledonian–Early Hercynian in the EKOB and a basis for the evolution of the Proto-Tethys in the EKOB.

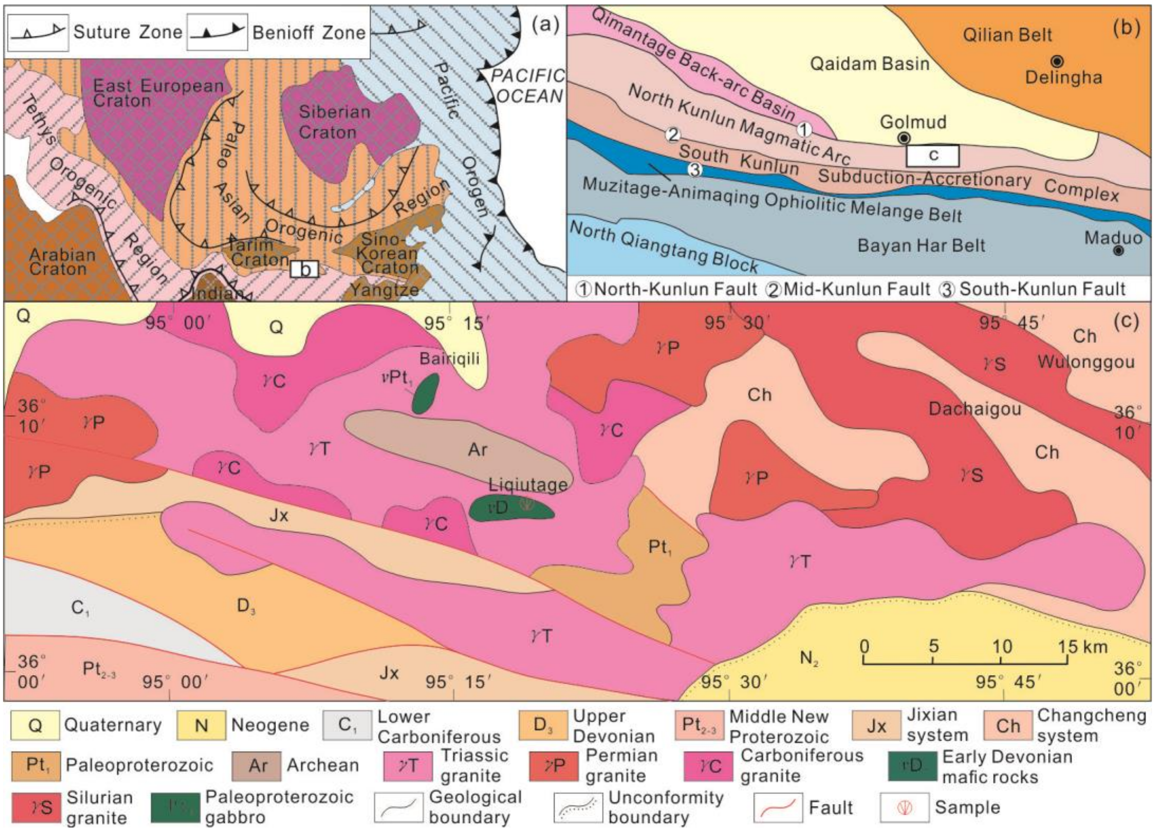

Figure 1. (**a**,**b**) Geotectonic location map. (**c**) Geological sketch of the Lichotag region in the EKOB ((**a**), modified from [41]; (**b**,**c**), after [42]).

2. Geological Background

The EKOB is divided into four major tectonic units: from north to south are the Qimantag back-arc basin, the North Kunlun magmatic arc, the South Kunlun subduction–accretionary mélange belt, and the Muzitag–A'nyemaqen ophiolite belt (Figure 1b). The Lichotag mafic intrusions are located in the North Kunlun magmatic arc. The base of this magmatic arc consists of the Precambrian, strongly metamorphosed Terran core mafic intrusions, the Paleo–Mesoproterozoic Jinshukou Group and the Xiaomiao Formation, and the Langyashan Formation. The epigenetic Uranian strata comprise mainly the Early Carboniferous Dagangou Formation sedimentary rocks and the Late Devonian Yaksan Formation terrestrial volcanic rocks (Figure 1c). The North Kunlun magmatic arc has experienced complex and multiple magmatism, with magmatic rocks of different ages and genesis. Magmatism was weak in the Cambrian–Early Silurian. In the Carboniferous–

Triassic, magmatic activities associated with the closure of the Paleo-Tethys reached the peak and formed the most widely distributed granites, followed by granites associated with the collisional orogeny in the Late Silurian–Devonian (432–376 Ma) [7–19,31–40,43–51]. The rocks are generally distributed in a NW direction, consistent with the regional structures, suggesting that they are controlled by the regional tectonic evolution.

3. Petrography

The Lichotag mafic intrusions are located in the southeast of Golmud City of Qinghai Province. The mafic intrusions are nearly oval in shape, about 6 km-long and 2 km-wide, with a long axis in the east–west direction and intruded by Triassic granites (Figure 1c). The mafic intrusions are mainly gabbro and diabase, and the boundaries between different lithologies are not obvious, with most showing gradual transition (Figure 2). In this study, gabbro (LQ03) and diabase (LQ04) samples were taken from fresh rock outcrops in the Lichotag region for analysis.

Figure 2. Photographs of the contact between Lichotag mafic intrusion in the EKOB.

The gabbro is dark gray–green and mainly consists of plagioclase (52%), pyroxene (45%) (Figure 3a), and a small number of dark minerals (about 3%). Plagioclase is medium to fine-grained and subhedral in shape. It develops Carlsbad–albite compound twinning and albite twinning, mostly being labradorite. Pyroxene consists of subhedral, short columnar, and hypidiomorphic–allomorphic grains of 0.4–3 mm in size, mainly medium to fine grains. It is light brownish green with high positive reliefs and two groups of cleavages. It is mostly augite and enstatite and often alters into chlorite, biotite, calcite, etc. Both pyroxene and plagioclase are subhedral and formed simultaneously, representative of a typical gabbro texture.

The diabase is dark gray–green and exhibits a typical diabase structure and almond structure, as a whole. It consists of plagioclase (50%), pyroxene (43%) (Figure 3b), a small amount of amygdale (6%) (Figure 3c,d), and dark minerals (1%). Plagioclase is subhedral platy with mainly fine-grained particles of 0.1–0.48 mm in size. Polysynthetic twinning is commonly developed. Pyroxene consists of subhedral, short columnar, and subhedral to anhedral grains sized 0.04–0.25 mm, mainly slightly chloritized fine grains. The pyroxene grains fill the triangular space formed by plagioclase, showing a typical diabase texture. The core of amygdale is mostly filled with calcite and chlorite. The chlorite has undulose extinction with abnormal indigo and rusty interference colors. Some secondary veins can be seen cutting through the amygdale.

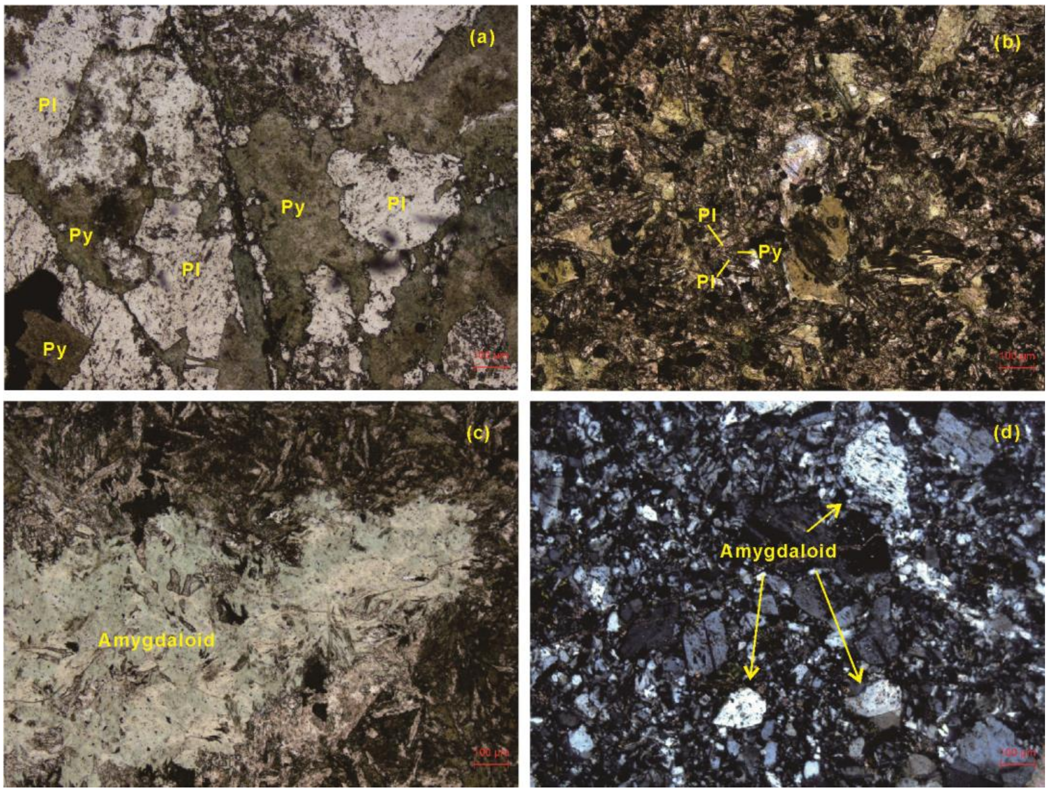

Figure 3. Micrographs of Lichotag mafic intrusion in the EKOB. (**a**) Micrographs of gabbro (sample LQ03). (**b**) Micrographs of diabase (sample LQ04). (**c**,**d**) Micrographs of amygdale in diabase (sample LQ04). Pl = Plagioclase, Py = Pyroxene.

4. Analytical Methods

4.1. LA–ICP–MS Testing

Zircons were collected from gabbroic clasts in the Lichotag mafic intrusions. The sampling locations of the two samples were 36°6′47.7″ N and 95°18′59.3″ E (Figure 1c). The weight of each sample was 30 kg. Samples were cleaned and crushed to 80–100 mesh for extraction of zircons by conventional heavy-liquid and electromagnetic separation. Zircons were selected manually under a binocular microscope. Those with good crystal shapes and high transparency without inclusions or cracks were chosen for analysis. The selected zircons were embedded in epoxy resin and polished to expose their interiors. Then, after using transmitted light and reflected light microscopy and cathodoluminescence (CL) to reveal the internal structure of the zircons to help select the optimal testing site, we performed laser ablation–inductively coupled plasma–mass spectrometry (LA–ICP–MS) analysis on the properly chosen sites.

The CL, LA–ICP–MS, and micro-area U–Pb dating of zircon were completed at the Testing Center of the Xi'an Institute of Geology and Mineral Resources. The experiment was carried out by using an Agilent 7500 ICP–MS, a COMPex 102 ArF excimer laser (working material ArF, wavelength 193 nm, 30 μm-diameter laser-beam spot, 20–40 μm depth of ablation sample), of Lambda Physik company of Germany, and the Geolas 200 M optical system of the Micro-Las company. In the experiment, He was used as the carrier gas and NIST SRM 610, a synthetic silicate-glass reference material developed by the National Institute of Standards and Technology, was used to optimize the instrument. The sampling method used was single-point erosion, and the data-acquisition method was based on one mass peak and one point-jumping peak. The reference standard sample was analyzed once every six measuring-point determinations. Before and after the analysis of 12 zircons, NIST SRM 610 was measured twice. Standard zircon 91500 was used as the external standard for zircon age analyses, and Andersen's 3D coordinate method was used to correct the ordinary lead. Element contents were determined against NIST SRM 610 as the external standard and ^{29}Si as the internal standard. The isotopic ratio and element content data were analyzed using the ICPMS Data Cal software package (9.0 edition) [52]. The common lead correction was conducted using the Andersen software (3.15 edition) [53], and Isoplot software (3.0 edition) [54] was used for age calculation and concordia diagrams. The analytical methods and instrument settings used were the same as those reported by Li et al. [55].

4.2. Geochemical Analyses

Six gabbro samples and six diabase samples were collected for chemical analysis. The samples were analyzed at the Key Laboratory of Magmatism and Mineralization Continental Dynamics, Ministry of Natural Resources, and the analytical data are shown in Supplementary Table S2. The sample loss-on-ignition (LOI) ranged from 3.32 wt.% to 4.11 wt.%, and some samples were affected by late alteration. The oxide content was recalculated after normalizing the sample data by deducting the loss-on-ignition.

5. Results

The zircon U-Pb isotope data and whole-rock geochemistry for the Lichotag mafic intrusions are listed in Supplementary Tables S1 and S2.

5.1. Zircon U-Pb Age

The CL image (Figure 4) shows that the zircons of the mafic intrusions are mostly euhedral or subhedral equigranular or stubby. Zircons are roughly categorized into two types. The first type has a homogeneous internal structure and clear oscillatory zoning, with most of medium-width equigranular or short columnar. The sizes of zircon grains in gabbro mostly range from 50 to 80 μm, with a few larger ones exceeding 100 μm, while zircon grains in diabase mostly range from 40 to 70 μm, with a few larger ones reaching 100 μm. All zircons show magmatic textures with Th/U ratios ranging from 0.02 to 1.74. The $^{206}Pb/^{238}U$ ages of 17 zircons from the gabbro range from 409.9 $\pm$ 4.28 Ma to 412.1 $\pm$ 3.64 Ma, and all the data fall on the concordia (Figure 5b). Their weighted mean age is 408.9 $\pm$ 2.0 Ma (MSWD = 0.49) (Figure 5c), representing an Early Devonian crystallization age of the gabbro. The $^{206}Pb/^{238}U$ ages of six zircons of the diabase range from 403.9 $\pm$ 3.73 Ma to 416.9 $\pm$ 6.85 Ma, and the data fall near the concordia, showing lead loss (Figure 5e). Their weighted average age is 411.1 $\pm$ 3.1 Ma (MSWD = 0.044) (Figure 5f), also suggesting an Early Devonian crystallization age of the diabase. The other type of zircons has obvious oscillatory bands, irregular morphologies, and diverse internal structures (Figure 4). The $^{206}Pb/^{238}U$ ages range from 684.1 $\pm$ 5.7 Ma to 3005.4 $\pm$ 31.74 Ma, indicating the complex origin of zircons, which were captured during the intrusion of gabbro and diabase, probably from the Precambrian basement of the North Kunlun magmatic arc.

5.2. Major and Trace Element Geochemistry

Major rare earth elements (REE) and trace element data and calculated parameters for the 11 representative samples are listed in Supplementary Table S2. All samples exhibit relatively uniform major oxide compositions.

5.2.1. Major Elements

The gabbro and diabase samples belong to iron-rich mafic intrusions, with SiO_2 content ranging from 47.31 wt.% to 54.95 wt.%, TiO_2 content from 0.87 wt.% to 1.51 wt.%, Al_2O_3 content from 15.91 wt.% to 20.84 wt.%, MgO content from 5.53 wt.% to 6.53 wt.%, $Mg^{\#}$ values from 50.58 to 59.48, and $Fe_2O_3{}^T$ content from 7.68 wt.% to 11.59 wt.%. The $Na_2O + K_2O$ content of these rocks ranged from 3.47 wt.% to 5.45 wt.%, with an average value of 4.54 wt.%. The Na_2O/K_2O ratio of 1.39 to 3.09 indicates its sodium-rich and potassium-poor characteristics. In a Nb/Y-Zr/TiO_2 plot (Figure 6a), the samples lie in the tholeiite fields. In an AFM plot, the rocks fall into the calcium-base series region (Figure 6b).

Microscopically, the diabase is mainly composed of calcic plagioclase, augite, and enstatite, with a typical gabbroic structure (Figure 3b–d).

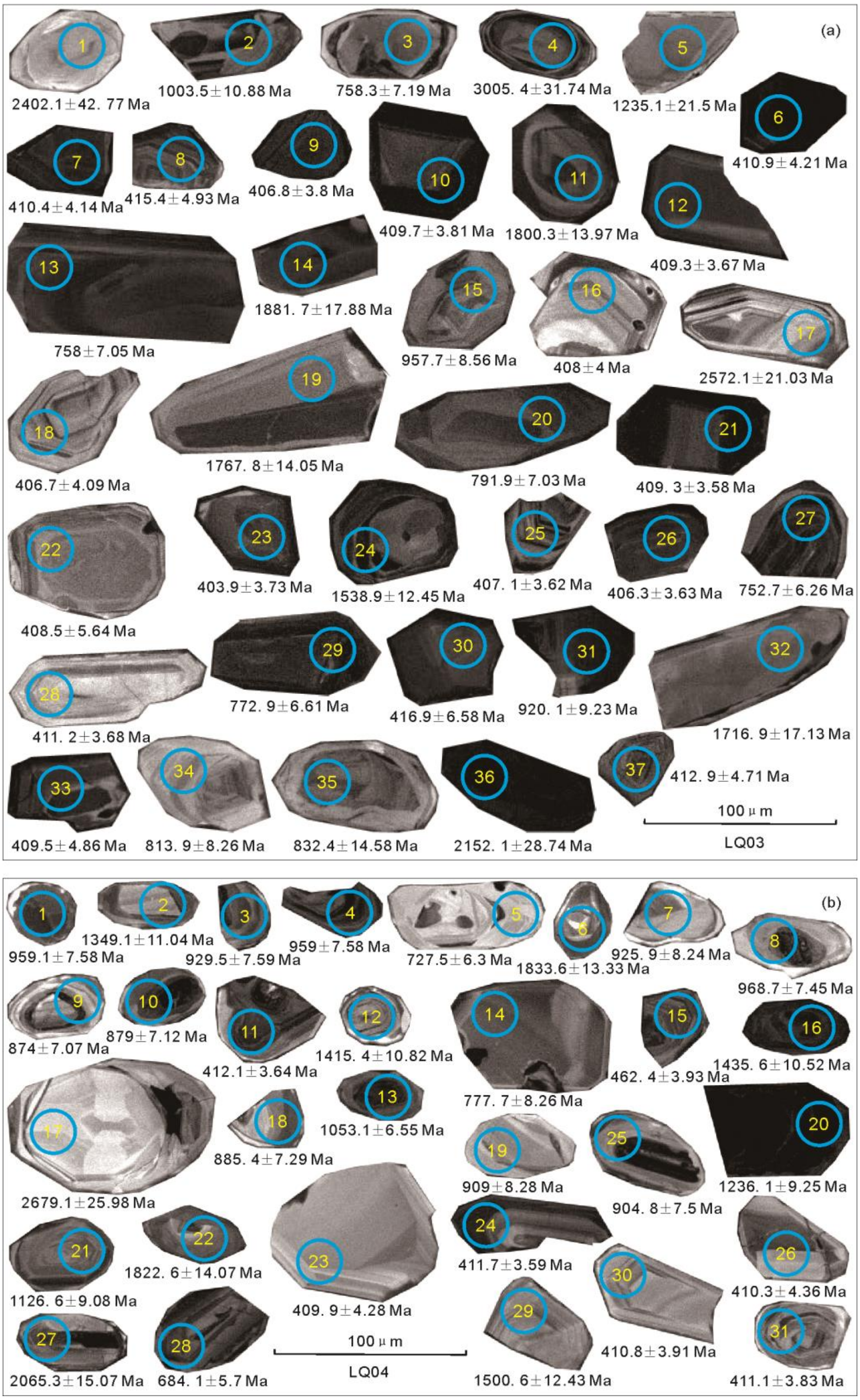

Figure 4. Zircon CL images of Lichotag mafic intrusion in the EKOB. (**a**) CL images of gabbro zircon (sample LQ03). (**b**) CL images of diabase zircon (sample LQ04).

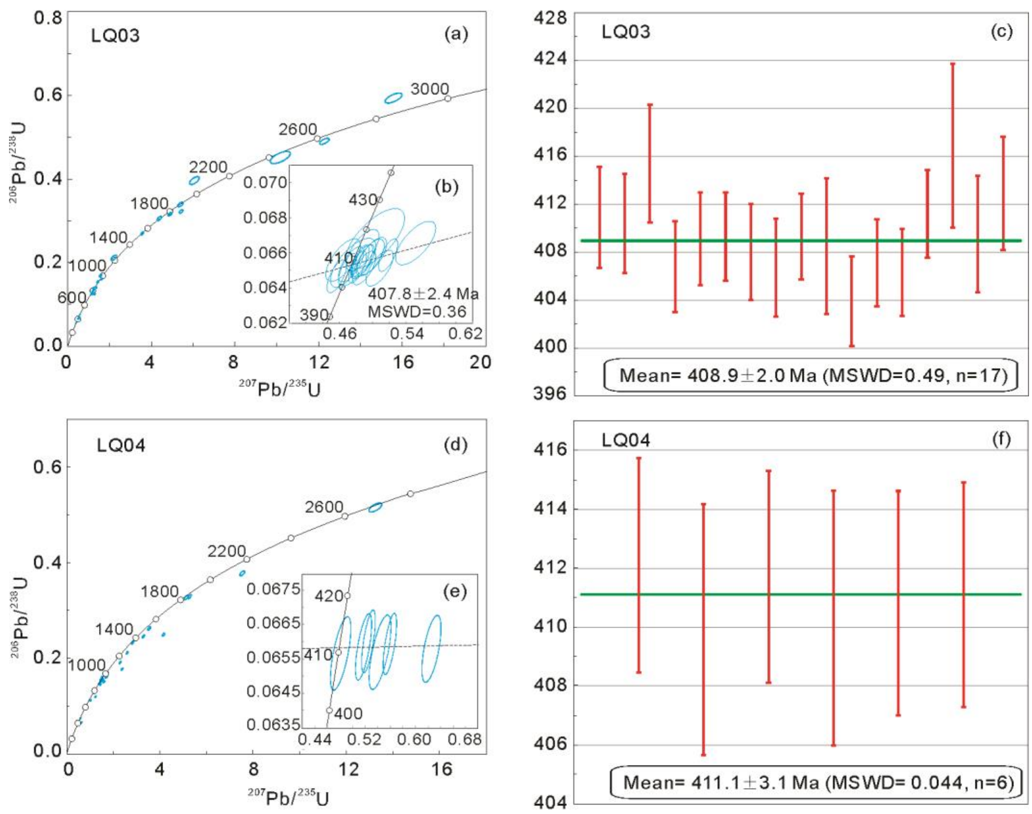

Figure 5. Concordia and weighted mean age plots (**a**–**f**) of LA–ICP–MS zircon U–Pb ages for Lichotag mafic intrusion in the EKOB.

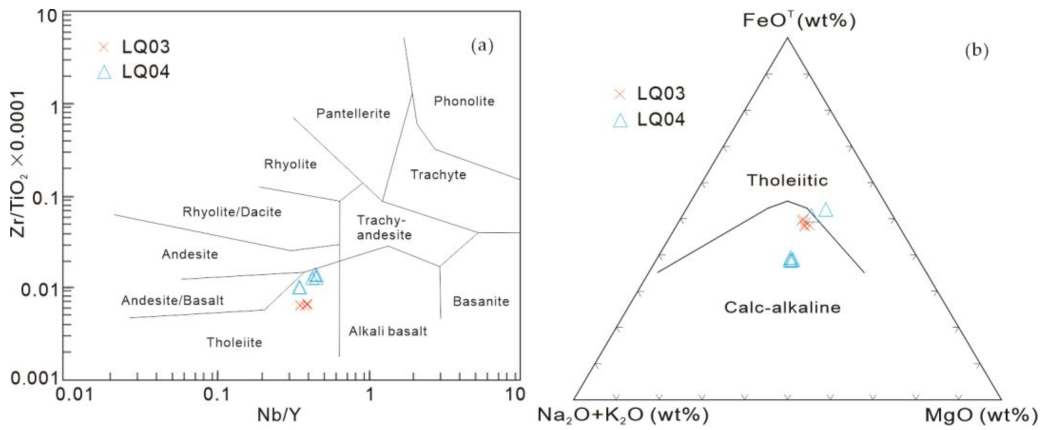

Figure 6. Nb/Y-Zr/TiO_2 (**a**) and AFM (**b**) plots of Lichotag mafic intrusion in the EKOB [56].

In general, the rocks are enriched in titanium, iron, and sodium, and depleted in magnesium and potassium. They belong to sodium-rich rocks, characterized by high iron and low magnesium contents.

5.2.2. Rare Earth Elements and Trace Elements

The total content of REE (ΣREE) of gabbro and diabase ranges from 64.53×10^{-6} to 151.24×10^{-6}. The chondrite-normalized REEs (Figure 7a) are characterized by obvious light and heavy REE fractionation and enrichment of LREE, with LREE/HREE = 3.83–7.71, $(La/Yb)_N$ = 3.27–6.75, δEu = 0.83–1.14, and no significant Europium anomaly. The primitive mantle-normalized [57] spider diagram of trace elements shows that the rocks are relatively enriched in Rb, U, Sr, and Nd, and relatively depleted in Nb, Ta, Ti, Zr, Hf, and Th (Figure 7b), showing characteristics of Th > Ta and La > Ta. The rocks also have low Cr and Ni contents (20.4 × 10^{-6} to 154 × 10^{-6} and 12.9 × 10^{-6} to 37.7 × 10^{-6}, respectively) and Sr/Y ratios of 17.3–22.5.

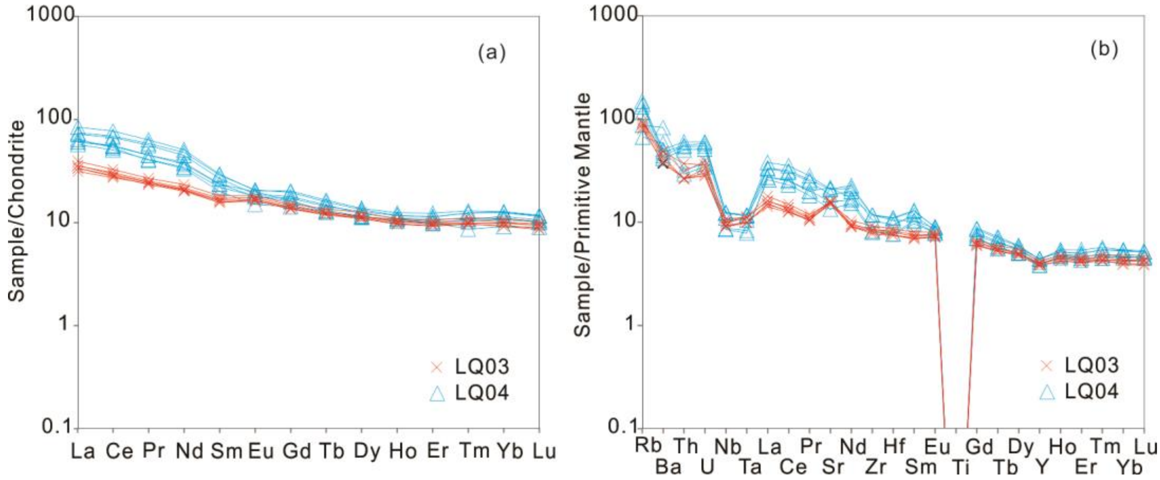

Figure 7. (**a**) Chondrite-normalized REE patterns. (**b**) Primitive mantle-normalized incompatible element distribution patterns for Lichotag mafic intrusion in the EKOB (chondrite data and primitive mantle data for normalization taken from Sun et al. [57]).

6. Discussion

6.1. Petrogenesis

The $Mg^{\#}$ of gabbro and diabase samples is 50.46–59.48. The low contents of compatible elements Cr and Ni suggest that the magma may not have undergone pyroxene stacking crystallization. The rocks have high Rb and Sr content (0.16–0.22) and are relatively enriched in Rb, U, Sr, and Nd, all of which show characteristics of the enriched mantle. The rocks have low Ce/Y ratios (1.21 to 3.15, with a mean value of 1.99), indicating that they may be from the spinel–garnet phase stability field [58]. In Figure 8a, most of the rock sample data fall in the spinel and garnet lherzolite phase field (closer to the spinel lherzolite phase), with partial melting of roughly 3% to 20%, suggesting that the mafic magma was probably derived from the spinel lherzolite phase, and the magma source region is deeper than 80 km [59].

As the mantle-derived magma intruded into the crust, it usually underwent different degrees of assimilation and mixing with the surrounding rocks. Zircon U–Pb dating results show that both gabbro and diabase have captured zircons formed in Neoproterozoic and Archaean (752–3005 Ma), which is the direct evidence of assimilation and mixing in this region. In addition, the rocks have low TiO_2 contents (<2 wt.%) and Zr/Nb (>13) [60,61]. Trace elements are characterized by Th > Ta, La > Ta, and depleted Nb and Ta. These results suggest some impacts of continental-crust mixing during magmatic evolution [62]. The $(La/Nb)_{PM}$–$(Th/Ta)_{PM}$ diagram (Figure 8b) shows that the crust materials involved in the miscibility are mainly from the upper crust, which is consistent with the Nb and Ta depletion in the gabbro. It is well-known that high La/Sm values (>4.5) indicate strong mixing of crust materials, while La/Sm < 2 indicates rarely mixed by crust materials [63]. Thus, the La/Sm values of 3.17–4.52 (with a mean value of 3.76) for the Lichotag mafic intrusions indicate that the mafic magma underwent some mixing, but to a strong degree. It should be noted that the mafic intrusions in this region are highly depleted in Nb and Ta. While it is possible that this depletion is related to assimilation and mixing, there is no clear correlation between the heterogeneity in assimilation and hybridization and the prevalence of Nb and Ta depletion in the mafic intrusions. Therefore, this depletion may also have been inherited from magma.

The gabbro and diabase are enriched in light rare earth elements (LREEs), showing significant fractionation between LREEs and heavy rare earth elements (HREEs). They are enriched in large ion lithophile elements such as Rb, U, Sr, and Nd, and relatively depleted in high-field-strength elements such as Nb, Ta, Zr, Hf, and Th. These features show the geochemical characteristics of magmatic rocks in island-arc environments [64]. Fractional crystallization does not affect the partition coefficients of Th, Nb, Zr, and Yb in the magma, so the ratios of these element pairs can also indicate the characteristics of the source region. Gabbro and diabase have high Th/Yb ratios (1.06–1.91), and the samples in the Nb/Yb–Th/Yb diagram (Figure 8c) all deviate significantly from the MORB–OIB evolutionary line and fall in the intra-oceanic-arc and land margin-arc areas, suggesting an island-arc-related environment. Meanwhile, all the samples in the Ta/Yb–Th/Yb diagram (Figure 8d) fall within the continental marginal-arc area, further suggesting that the tectonic background of gabbro and diabase generation was closely related to the island-arc environment.

In summary, we believe that the mafic magma originated from the partial melting of the enriched mantle, and that the source region inherited the accumulation of metasomatic fluids in the early oceanic subduction phase and was assimilated by the crust materials in the process of upward intrusion.

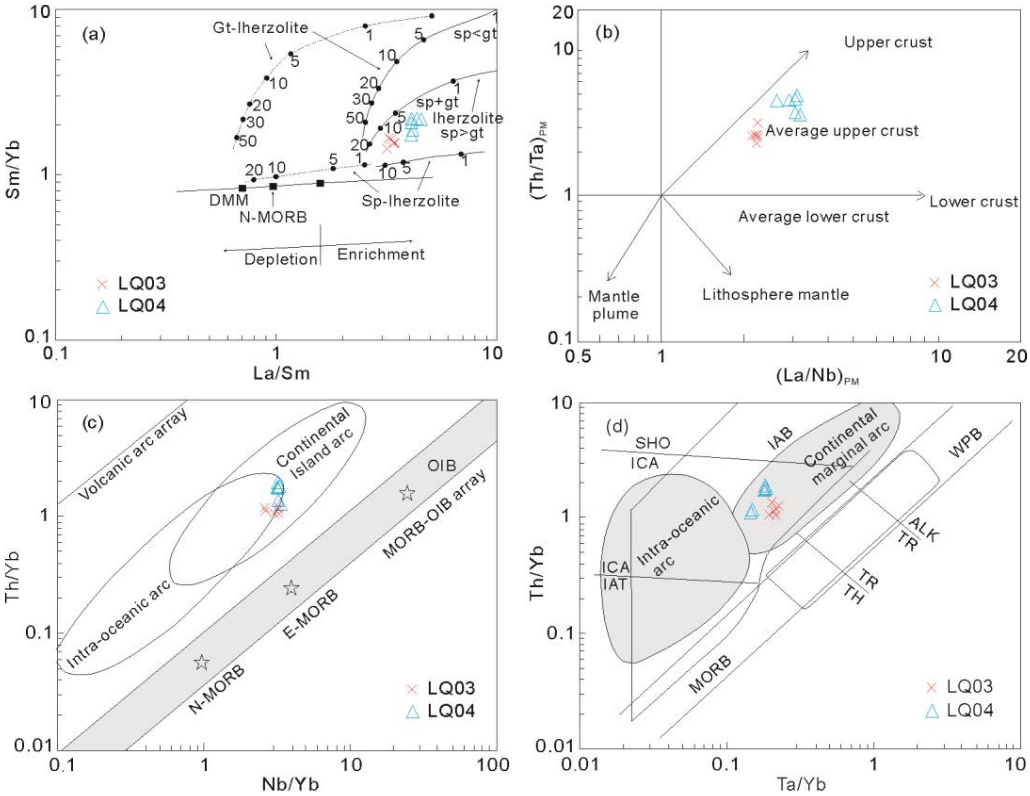

Figure 8. Plots of Sm/Yb–La/Sm (**a**) [65], $(La/Nb)_{PM}$–$(Th/Ta)_{PM}$ (**b**) [66], Nb/Yb–Th/Yb and Nb/Yb–Th/Yb (**c**) [65], and Ta/Yb–Th/Yb (**d**) [67] in Lichotag mafic intrusion in the EKOB. MORB stands for mid-ocean ridge basalts; N-MORB for normal MORB; E-MORB for enriched MORB; WPB for within-plate basalt; OIB for ocean island basalts; OIT for ocean island tholeiitic; OIA for ocean island alkaline; SHO for shoshonite; CAB for calc–alkaline basalts; ICA for island-arc calc–alkaline basalts; IAT for island-arc tholeiitic; IAB for island-arc alkaline basalts.

6.2. Geotectonic Setting and Geological Significance

The East Kunlun region is an important part of the Central orogenic belt [1–6], and studies have shown that the subduction of Neoproterozoic–Early Paleozoic Proto-Tethys and subduction of the Late Carboniferous–Triassic Paleotethys Ocean are the two most important orogenic events in this region, which have established the present-day tectonic pattern of the East Kunlun region [1–15]. Therefore, the study of the Paleozoic tectonic evolution of the East Kunlun region is important for the study of the tectonic evolution of the Proto-Tethys.

Petrological and geochemical studies of Lichotag mafic intrusion in the EKOB shows a calc–alkaline series with Nb and Ta depletions, consistent with the characteristics of mafic intrusions formed during a post-collisional extensional phase [62]. Magmatic rocks formed in a post-collisional extensional environment exhibit geochemical characteristics of island-arc magmatic rocks or active continental margin magmatic rocks. They are enriched in Rb, U, Sr, Nd, etc., and depleted in Nb and Ta, characteristics of island-arc magmatic rocks. In the Hf/3–Th–Ta diagram (Figure 9a), they fall into the continental margin-arc calc–alkaline basalt region, showing the metasomatism of subduction fluids. They show characteristics of volcanic-arc basalts in the Nb×2–Zr/4–Y diagram (Figure 9b) and fall into a volcanic-arc basalt region in the Hf/3–Th–Nb/16 diagram (Figure 9c). Meanwhile, they are clearly distinguished from N-type mid-ocean ridge basalts in the illustrated area.

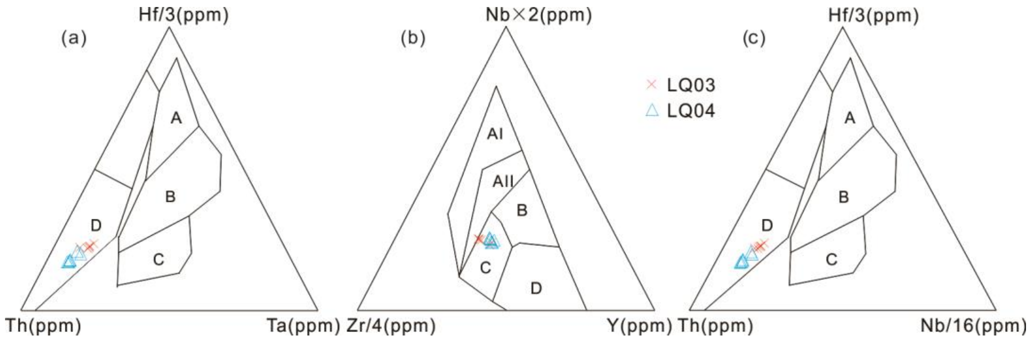

Figure 9. Plots of Lichotag mafic intrusion gabbro and diabase Hf/3–Th–Ta (**a**) [68], Nb × 2–Zr/4–Y (**b**) [69], and Hf/3–Th–Nb/16 (**c**) [68] in the EKOB. Hf/3–Th–Ta diagram: A—depleted mid-ocean ridge basalts, B—enriched mid-ocean ridge basalts and within-plate tholeiitic, C—within-plate tholeiitic, D—volcanic-arc basalts. Nb × 2–Zr/4–Y diagram: AI—within-plate alkaline basalts, AII—within-plate alkaline basalts and within-plate tholeiitic, B—E-MORB, C—within-plate tholeiitic and volcanic-arc basalts, D—depleted MORB and volcanic-arc basalts. Hf/3–Th–Nb/16 diagram: A—depleted MORB, B—E-MORB and within-plate tholeiitic, C—within-plate tholeiitic, D—volcanic-arc basalts.

The East Kunlun Ocean is located between the Qaidam Block and the Bayan Hara Block. Starting from Late Neoproterozoic, the East Kunlun Ocean Basin subducted along the center of East Kunlun, forming the Cambrian–Ordovician Ayaikekumu Lake subduction accretionary complex, which contains ophiolitic mélange and the Cambrian Ocean island–seamount volcanic–sedimentary assemblage. The subduction of the eastern section of the ocean basin was slightly later than that of the western section along the Ayaikekumu Lake, and the subduction accretionary complex belt was formed in the Early Paleozoic. This subduction accretionary complex belt contains volcanic rocks, carbonates, sandstones, and marbles, as well as tectonic slices of the Early Paleozoic in addition to ophiolitic mélange, among which the volcanic rocks and carbonates may be the products of the breakup of oceanic seamounts and islands [2,5,6,70]. With the continuous subduction of the oceanic crust, a large number of arc magmatic rocks formed in the region, which are mainly diorites and a few gabbroic rocks, such as high-Mg andesite (519 ± 4.2 Ma) [71] and diorite (513.8 ± 2.9 Ma) [71] in the Lalung Gauri River region, diorite (510.4 ± 3 Ma) [72] and ultramafic–mafic intrusions (509 ± 7 Ma) [73] in the DulanKeke sand region, and Yaziquan diorite (480 ± 3 Ma) [74], Zhiyu North monzodiorite (464.6 ± 1.9 Ma) [72], Wanggaxiu gabbro (468 ± 2 Ma) [74], Ulan–Uzul biotite granite (457.5 ± 2.3 Ma) [75], Achaodun quartz diorite (448.8 ± 3.9 Ma) [76], etc. In addition, some metamorphic events in this region also indicate the existence of oceanic crust subduction. For example, the Qingshuiquan granulites of the central East Kunlun Suture Zone (507 Ma) were formed by high-temperature and medium-pressure granulite facies metamorphism during the subduction of the oceanic lithosphere [77]. The Heiyun biotite feldspar gneisses of the Jinshukou

Group in the southern part of Nomukhong were formed by island-arc-type low-pressure amphibolite-granulite facies metamorphism in the north of EKOB at 460 Ma [78]. The Huxiaoqin mafic rocks (438 ± 2 Ma) [79] and the Qingshuiquan mafic veins (436.4 ± 1.2 Ma) [37] with island-arc basalt characteristics in the central suture zone of East Kunlun represent the most recent magmatic records of oceanic crust subduction in this region. Eclogites are exposed along the Xiaozaohuo–Suhaitu–Xiarihamu–Laningzaohuo Belt of the EKOB, with intermittent extensions of up to 20 km. These eclogites are mainly hosted in the Neoarchean–Paleoproterozoic Baishahe Complex (Ar_3Pt_1B), with metamorphic ages of 436–415 Ma. The presence of terrigenous crust eclogites represents the closure of the central East Kunlun Ocean Basin [37,40,80–83]. The prograde metamorphic age of eclogites is 436–415 Ma and its retrograde metamorphic age is 415–390 Ma. The former age was related to the collisional extrusion environment, while the latter age corresponds to an extensional environment, which also indirectly constrains the closure time of the central East Kunlun Ocean Basin.

The ages of the granites and diorites associated with the continent–continent collision in the Qimantag region are 428.5 ± 2.2 Ma and 430.8 ± 1.7 Ma, respectively [84], whereas A-type granites began to appear in the region at 430 Ma ± [85], consistent with the timing of the high-pressure eclogite facies metamorphism at 428 Ma in the central East Kunlun [80] and the medium-pressure amphibolite facies metamorphism at 427 Ma [8]. This indicates that the intensive continent–continent collisional period in the region started to cease at 428 Ma and the post-collisional extension in the East Kunlun region continued into the Late Devonian. During this period, the magmatic rocks in the East Kunlun region were mainly A-type granites, peraluminous–strongly peraluminous granites, Mg-rich diorite, and gabbro. Bimodal intrusive rocks are widely developed in the region, such as the A-type granite of Baiganhu (430–429 Ma) [86], the Ulan–Uzur monzogranite (422.5 ± 1.6 Ma) [87], the Xiazhamu gabbro–norite (423 ± 1 Ma) [88], Hongqigou A-type syenogranite (420 ± 3 Ma) [89], Balong diorite porphyrite (420 ± 3 Ma) [90], Yazigou monzodiorite (415.5 ± 2.6 Ma) [91], Xiaoyuanshan gabbro (415 ± 16 Ma) [92], Wulonggou gabbro (410.3 ± 2.7 Ma) and alkali granite (410.5 ± 1.8 Ma) [93], Jinshukou diorite (405 ± 3 Ma) [28], Binggou syenogranite (391 ± 3 Ma) [94], and Qimantag Kayakden Tag district granodiorite (380.52 ± 0.92 Ma) [95]. All these formation ages are consistent with the formation timeframe of 423–406 Ma for the extensional molasse construction of the Yakshan Group [4,96]. All the above features suggest a typical post-collisional extensional tectonic setting for the East Kunlun region.

Therefore, we believe that the Lichotag mafic intrusions are along with the continuous subduction of the Proto-Tethys in the Late Caledonian. The subducting slab was de-hydrated and replaced the overlying mantle wedge during the subduction process, forming a locally enriched mantle end member with subduction components. After the end of the Late Caledonian–Early Hercynian subduction, the enriched mantle end member was dismantled and sunk in the post-collisional extensional environment. This then triggered the partial melting and upwelling of the enriched lithospheric mantle with the characteristics of subduction components to form the mafic magma [97–99]. The mafic magma was assimilated during the upwelling process to form gabbro and diabase by intrusion into the upper crust.

7. Conclusions

The comprehensive study of the Lichotag mafic intrusions in the EKOB based on petrological, geochronological, and geochemical have led to the following conclusions:

(1) The Lichotag mafic intrusion was formed in the Early Devonian, with a zircon U–Pb age of 408.9 ± 2.0 Ma (MSWD = 0.49) for gabbro and a zircon U–Pb age of 411.1 ± 3.1 Ma (MSWD = 0.044) for diabase.

(2) The chondrite-normalized curves of REEs in gabbro and diabase showed similar patterns with enrichment of LREEs and insignificant europium anomaly. The rocks are characterized by low contents of compatible elements Cr and Ni, high Rb and Sr

contents, enrichment of large-ion lithophile elements such as Rb, U, Sr, and Nd, and relatively depleted high-field-strength elements such as Nb, Ta, Zr, Hf, Th, etc. The mafic magma originated from the enriched mantle and was assimilated by the upper crust during magma ascent.

(3) The Lichotag mafic intrusions in the EKOB were formed in a post-collisional extensional tectonic regime, indicating that the subduction of the Proto-Tethys ended in the Early Devonian and the East Kunlun region was in a post-collisional extensional tectonic environment.

Supplementary Materials: The following supporting information can be downloaded at: https://www.mdpi.com/article/10.3390/min13040478/s1, Table S1: Zircon LA–ICP–MS U–Pb data of the gabbro and diabase in the Lichotag. Table S2: Whole-rock major and trace element data of the gabbro and diabase in the Lichotag.

Author Contributions: Conceptualization, Y.M., X.Z. and Z.L.; methodology, Y.M. and X.Z.; software, Y.H. and Y.Y.; validation, Y.M., X.Z. and H.Z.; formal analysis, Y.M., X.Z. and Z.L.; investigation, Y.M., X.Z., H.Z., Y.H., Y.Y. and X.X.; resources, Y.M. and X.Z.; data curation, Y.M. and X.Z.; writing—original draft preparation, Y.M.; writing—review and editing, Y.M., X.Z. and Z.L.; visualization, Y.M.; supervision, Y.M. and X.Z.; project administration, Y.M.; funding acquisition, Y.M. and X.Z. All authors have read and agreed to the published version of the manuscript.

Funding: This research was funded by the National Natural Sciences Foundation of China (Grant No. 41872235) and the China Geological Survey (Grant Nos. DD20190364, DD20220978).

Data Availability Statement: The original contributions presented in the study are included in the article/Supplementary Materials.

Acknowledgments: Thanks are extended to the chief editor and the two anonymous reviewers for their constructive reviews, which have greatly improved our manuscript.

Conflicts of Interest: The authors declare no conflict of interest.

References

1. Xu, Z.Q.; Yang, J.S.; Jiang, M.; Li, H.B.; Xue, G.Q.; Yuan, X.C.; Qian, H. Deep structure and lithospheric shear faults in the east Kunlun–Qiangtang region, northern Tibetan Plateau. *Sci. China Ser. D Earth Sci.* **2001**, *44*, 1–9. [CrossRef]
2. Yu, M.; Dick, J.M.; Feng, C.Y.; Li, B.; Wang, H. The tectonic evolution of the East Kunlun Orogen, northern Tibetan Plateau: A critical review with an integrated geodynamic model. *J. Asian Earth Sci.* **2020**, *191*, 104168. [CrossRef]
3. Zhang, J.X.; Yu, S.Y.; Mattinson, C.G. Early Paleozoic polyphase metamorphism in northern Tibet, China. *Gondwana Res.* **2017**, *41*, 267–289. [CrossRef]
4. Dong, Y.P.; He, D.F.; Sun, S.S.; Liu, X.M.; Zhou, X.H.; Zhang, F.F.; Yang, Z.; Cheng, B.; Zhao, G.C.; Li, J.H. Subduction and accretionary tectonics of the East Kunlun orogen, western segment of the Central China Orogenic System. *Earth-Sci. Rev.* **2018**, *186*, 231–261. [CrossRef]
5. Dong, Y.P.; Sun, S.S.; Santosh, M.; Zhao, J.; Sun, J.P.; He, D.F.; Shi, X.H.; Hui, B.; Cheng, C.; Zhang, G.W. Central China Orogenic Belt and amalgamation of East Asian continents. *Gondwana Res.* **2021**, *100*, 131–194. [CrossRef]
6. Dong, Y.P.; Hui, B.; Sun, S.S.; Yang, Z.; Zhang, F.F.; He, D.F.; Sun, J.P.; Shi, X.H. Multiple orogeny and geodynamics from Proto–Tethys to Paleo–Tethye of the Central China Orogenic Belt. *Acta Geol. Sin.* **2022**, *96*, 3426–3448. (In Chinese with English Abstract)
7. Liu, C.D.; Mo, X.X.; Luo, Z.H.; Yu, X.H.; Chen, H.W.; Li, S.W.; Zhao, X. Mixing events between the crust- and mantle-derived magmas in Eastern Kunlun: Evidence from zircon SHRIMP II chronology. *Chin. Sci. Bull.* **2004**, *49*, 828–834. [CrossRef]
8. Chen, N.S.; Sun, M.; Wang, Q.Y.; Zhang, K.X.; Wan, Y.S.; Chen, H.H. U-Pb dating of zircon from the central zone of the east Kunlun orogen and its implications for tectonic evolution. *Sci. China Ser. D Earth Sci.* **2008**, *51*, 929–938. [CrossRef]
9. Li, Z.C.; Pei, X.Z.; Li, R.B.; Pei, L.; Liu, C.J.; Chen, Y.X.; Liu, Z.Q.; Chen, G.C.; Xu, T.; Yang, J.; et al. Geochronology, Geochemistry and Tectonic Setting of the Bairiqiete Granodiorite Intrusion (Rock Mass) from the Buqingshan Tectonic Melange Belt in the Southern Margin of East Kunlun. *Acta Geol. Sin.* **2014**, *88*, 584–597. [CrossRef]
10. Xiong, F.H.; Ma, C.Q.; Jiang, H.A.; Liu, B.; Huang, J. Geochronology and geochemistry of middle Devonian mafic dykes in the East Kunlun orogenic belt, northern Tibet Plateau: Implications for the transition from Prototethys to Paleotethys orogeny. *Geochemistry* **2014**, *74*, 225–235. [CrossRef]
11. Xiong, F.H.; Ma, C.Q.; Wu, L.; Jiang, H.A.; Liu, B. Geochemistry, zircon U-Pb ages and Sr-Nd-Hf isotopes of an Ordovician appinitic pluton in the East Kunlun orogen: New evidence for Proto–Tethyan subduction. *J. Asian Earth Sci.* **2015**, *111*, 681–697. [CrossRef]

12. Zhao, X.; Fu, L.B.; Wei, J.H.; Bagas, L.; Santosh, M.; Liu, Y.; Zhang, D.H.; Zhou, H.Z. Late Permian back-arc extension of the eastern Paleo–Tethys Ocean: Evidence from the East Kunlun Orogen, Northern Tibetan Plateau. *Lithos* **2019**, *340–341*, 34–48. [CrossRef]
13. Chen, J.J.; Fu, L.B.; Wei, J.H.; Selby, D.; Zhang, D.H.; Zhou, H.Z.; Zhao, X.; Liu, Y. Proto–Tethys magmatic evolution along northern Gondwana: Insights from Late Silurian–Middle Devonian A–type magmatism, East Kunlun Orogen, Northern Tibetan Plateau, China. *Lithos* **2020**, *356–357*, 105304. [CrossRef]
14. Kong, J.J.; Niu, Y.L.; Hu, Y.; Zhang, Y.; Shao, F.L. Petrogenesis of the Triassic granitoids from the East Kunlun Orogenic Belt, NW China: Implications for continental crust growth from syn-collisional to post-collisional setting. *Lithos* **2020**, *364–365*, 105513. [CrossRef]
15. Zhou, H.Z.; Zhang, D.H.; Wei, J.H.; Wang, D.Z.; Santosh, M.; Shi, W.J.; Chen, J.J.; Zhao, X. Petrogenesis of Late Triassic mafic enclaves and host granodiorite in the Eastern Kunlun Orogenic Belt, China: Implications for the reworking of juvenile crust by delamination-induced asthenosphere upwelling. *Gondwana Res.* **2020**, *84*, 52–70. [CrossRef]
16. Li, R.B.; Pei, X.Z.; Li, Z.C.; Pei, L.; Chen, Y.X.; Liu, C.J.; Chen, G.C.; Feng, K. Geochemistry and tectonic setting of Middle Ordovician MORB-like basalts in the Kunlun Orogen: Implications for a back-arc environment. *Arab. J. Geosci.* **2021**, *14*, 395. [CrossRef]
17. Chen, G.C.; Pei, X.Z.; Li, R.B.; Li, Z.C.; Chen, Y.X.; Liu, C.J.; Pei, L. Multiple sources of Indosinian granites and constraints on the tectonic evolution of the Paleo–Tethys Ocean in East Kunlun Orogen. *Minerals* **2022**, *12*, 1604. [CrossRef]
18. Li, Z.C.; Pei, X.Z.; Bons, P.D.; Li, R.B.; Pei, L.; Chen, G.C.; Chen, Y.X.; Liu, C.J.; Wang, M.; Zhao, S.W.; et al. Petrogenesis and tectonic setting of the early-middle Triassic subduction-related granite in the eastern segment of East Kunlun: Evidences from petrology, geochemistry, and zircon U-Pb-Hf isotopes. *Int. Geol. Rev.* **2022**, *64*, 698–721. [CrossRef]
19. Li, R.B.; Pei, X.Z.; Zhou, R.J.; Li, Z.C.; Pei, L.; Chen, G.C.; Chen, Y.X.; Liu, C.J. Magmatic response to the closure of the Proto–Tethys Ocean: A case study from the middle Paleozoic granitoids in the Kunlun Orogen, western China. *J. Asian Earth Sci.* **2023**, *242*, 105513. [CrossRef]
20. Mo, X.X.; Luo, Z.H.; Deng, J.F.; Yu, X.H.; Liu, C.D.; Chen, H.W.; Yuan, W.M.; Liu, Y.H. Granitoids and crustal growth in the East–Kunlun orogenic belt. *Geol. J. China Univ.* **2007**, *13*, 403–414. (In Chinese with English Abstract)
21. Yang, J.S.; Robinson, P.T.; Jiang, C.F.; Xu, Z.Q. Ophiolites of the Kunlun mountains, China and their tectonic implications. *Tectonophysics* **1996**, *258*, 215–231. [CrossRef]
22. Bian, Q.T.; Li, D.H.; Pospelov, L.; Yin, L.; Zhao, D.; Chang, D.; Luo, X.; Gao, S.; Astrakhantsev, O. Age, geochemistry and tectonic setting of Buqingshan Ophiolites, North Qinghai–Tibet plateau, China. *J. Asian Earth Sci.* **2004**, *23*, 577–596. [CrossRef]
23. Du, W.; Jiang, C.Y.; Xia, M.Z.; Xia, Z.D.; Zhou, W.; Ling, J.L.; Wang, B.Y. A newly discovered Early Paleozoic ophiolite in Dagele, Eastern Kunlun, China, and its geological significance. *Geol. J.* **2017**, *52*, 425–435. [CrossRef]
24. Peng, Y.B.; Yu, S.Y.; Li, S.Z.; Zhang, J.X.; Liu, Y.J.; Li, Y.S.; Santosh, M. Early Neoproterozoic magmatic imprints in the Altun–Qilian–Kunlun region of the Qinghai–Tibet Plateau: Response to the assembly and breakup of Rodinia supercontinent. *Earth-Sci. Rev.* **2019**, *199*, 102954. [CrossRef]
25. Li, R.B.; Pei, X.Z.; Wei, B.; Li, Z.C.; Pei, L.; Chen, G.C.; Chen, Y.X.; Liu, C.J. Middle Cambrian–Early Ordovician ophiolites in the central fault of the East Kunlun Orogen: Implications for an epicontinental setting related to Proto–Tethyan Ocean subduction. *Gondwana Res.* **2021**, *94*, 243–258. [CrossRef]
26. Li, Z.C.; Pei, X.Z.; Li, R.B.; Bons, P.D.; Pei, L.; Chen, Y.X.; Liu, C.J.; Wang, M.; Zhao, S.W.; Chen, G.C.; et al. Petrogenesis and tectonic setting of Early Silurian island-arc-type quartz diorite at the southern margin of the East Kunlun orogenic belt: Analysis of the evolution of the Proto–Tethyan Ocean. *Int. J. Earth Sci.* **2022**, *111*, 2317–2335. [CrossRef]
27. Chen, Y.X.; Pei, X.Z.; Li, Z.C.; Li, R.B.; Liu, C.J.; Wang, M. Magmatic events recorded in granitic gneisses from the Hatu area, eastern East Kunlun Orogen: Response to the assembly of Rodinia. *Geol. J.* **2017**, *52*, 403–418. [CrossRef]
28. Du, W.; Jiang, C.Y.; Tang, Z.l.; Xia, M.Z.; Xia, Z.D.; Ling, J.L.; Zhou, W.; Wang, B.Y. Discovery and zircon SHRIMP U-Pb ages of the Dagele eclogite from East Kunlun, Western China and the new constrains on the Central Kunlun suture zone. *Acta Geol. Sin.* **2017**, *91*, 1153–1154. [CrossRef]
29. Li, R.B.; Pei, X.Z.; Wei, B.; Li, Z.C.; Pei, L.; Chen, Y.X.; Liu, C.J.; Cheng, G.C.; Wang, M.; Feng, K. Constraints of late Cambrian mafic rocks from the Qushi'ang ophiolite on a back-arc system in a continental margin, East Kunlun Orogen, Western China. *J. Asian Earth Sci.* **2019**, *169*, 117–129. [CrossRef]
30. Li, R.B.; Pei, X.Z.; Li, Z.C.; Sun, Y.; Feng, J.Y.; Pei, L.; Chen, G.C.; Liu, C.J.; Chen, Y.X. Geochemical features, age, and tectonic significance of the Kekekete mafic-ultramafic rocks, East Kunlun Orogen, China. *Acta Geol. Sin.* **2013**, *87*, 1319–1333.
31. Chen, N.S.; Sun, M.; He, L.; Zhang, K.X.; Wang, G.C. Precise timing of the Early Paleozoic metamorphism and thrust deformation in the Eastern Kunlun Orogen. *Chin. Sci. Bull.* **2002**, *47*, 1130–1133. [CrossRef]
32. Zhu, Y.H.; Lin, Q.X.; Jia, C.X.; Wang, G.C. SHRIMP zircon U-Pb age and significance of early Paleozoic volcanic rocks in East Kunlun orogenic belt, Qinghai province, China. *Sci. China Ser. D Earth Sci.* **2006**, *49*, 88–96. [CrossRef]
33. Liu, B.; Ma, C.Q.; Huang, J.; Wang, L.X.; Zhao, S.Q.; Yan, R.; Sun, Y.; Xiong, F.H. Petrogenesis and tectonic implications of Upper Triassic appinite dykes in the East Kunlun orogenic belt, northern Tibetan Plateau. *Lithos* **2017**, *284–285*, 766–778. [CrossRef]
34. Pei, X.Z.; Li, R.B.; Li, Z.C.; Chen, Y.X.; Pei, L.; Liu, Z.Q.; Chen, G.C.; Li, X.B.; Wang, M. Composition feature and formation process of Buqingshan composite accretionary mélange belt in southern margin of East Kunlun Oragen. *Earth Sci.* **2018**, *43*, 4498–4520. (In Chinese with English Abstract)

35. Chen, N.S.; Sun, M.; Wang, Q.Y.; Zhao, G.C.; Chen, Q.; Shu, G.M. EMP chemical ages of monazites from central zone of the eastern Kunlun orogen: Records of multi-tectonometamorphic events. *Chin. Sci. Bull.* **2007**, *52*, 2252–2263. [CrossRef]
36. Li, R.B.; Pei, X.Z.; Li, Z.C.; Sun, Y.; Pei, L.; Chen, G.C.; Chen, Y.X.; Liu, C.J.; Wei, F.H. Regional tectonic transformation in East Kunlun orogenic belt in early Paleozoic: Constraints from the geochronology and geochemistry of Helegangnaren alkali-feldspar granite. *Acta Geol. Sin.* **2013**, *87*, 333–345.
37. Meng, F.C.; Zhang, J.X.; Cui, M.H. Discovery of Early Paleozoic eclogite from the East Kunlun, Western China and its tectonic significance. *Gondwana Res.* **2013**, *23*, 825–836. [CrossRef]
38. Li, Z.C.; Pei, X.Z.; Li, R.B.; Pei, L.; Liu, C.J.; Chen, Y.X.; Zhang, Y.M.; Wang, M.; Xu, T. Early Ordovician Island-arc-type Manite granodiorite pluton from the Buqingshan Tectonic Mélange Belt in the Southern margin of the East Kunlun: Constraints on subduction of the Proto–Tethyan Ocean. *Geol. J.* **2017**, *52*, 510–528. [CrossRef]
39. Li, R.B.; Pei, X.Z.; Li, Z.C.; Patias, D.; Su, Z.G.; Pei, L.; Chen, G.C.; Chen, Y.X.; Liu, C.J. Late Silurian to Early Devonian volcanics in the East Kunlun orogen, northern Tibetan Plateau: Record of postcollisional magmatism related to the evolution of the Proto–Tethys Ocean. *J. Geodyn.* **2020**, *140*, 101780. [CrossRef]
40. Wang, Q.; Zhao, J.; Zhang, C.L.; Yu, S.Y.; Ye, X.T.; Liu, X.Q. Paleozoic post-collisional magmatism and high-temperature granulite-facies metamorphism coupling with lithospheric delamination of the East Kunlun Orogenic Belt, NW China. *Geo. Sci. Front.* **2022**, *13*, 101271. [CrossRef]
41. Windley, B.F.; Alexeiev, D.; Xiao, W.J.; Kröner, A.; Badarch, G. Tectonic models for accretion of the Central Asian Orogenic Belt. *J. Geol. Soc.* **2007**, *164*, 31–47. [CrossRef]
42. Meng, Y.; Chen, F.N.; Yu, J.Y.; Ji, W.H.; Feng, Y.M.; Zhang, X.; Gu, P.Y.; Li, X.M.; Wang, K.; Zhu, X.H.; et al. *Tectonic Evolution in Northwest China and Its Adjacent Areas*; China University of Geosciences Press: Wuhan, China, 2022; pp. 73–194. (In Chinese)
43. Ba, J.; Zhang, L.; He, C.; Chen, N.S.; M. Kusky, T.; Wang, Q.Y.; Wan, Y.S.; Liu, X.M. Zircon and monazite ages constraints on Devonian magmatism an granulite-facies metamorphism in the Southern Qaidam block: Implications for evolution of Proto– and Paleo–Tethys in East Asia. *J. Earth Sci.* **2018**, *29*, 1132–1150. [CrossRef]
44. Ding, Q.F.; Song, K.; Zhang, Q.; Yan, W.; Liu, F. Zircon U-Pb geochronology and Hf isotopic constraints on the petrogenesis of the Late Silurian Shidonggou granite from the Wulonggou area in the Eastern Kunlun Orogen, North West China. *Int. Geol. Rev.* **2019**, *61*, 1666–1689. [CrossRef]
45. Li, L.; Sun, F.Y.; Li, B.L.; Li, S.J.; Chen, G.J.; Wang, W.; Yan, J.M.; Zhao, T.F.; Dong, J.; Zhang, D.X. Geochronology, geochemistry and Sr-Nd-Pb-Hf isotopes of No. I complex from the Shitoukengde Ni–Cu sulfide deposit in the Eastern Kunlun Orogen, Western China: Implications for the magmatic source, geodynamic setting and genesis. *Acta Geol. Sin.* **2018**, *92*, 106–126. [CrossRef]
46. Song, S.G.; Bi, H.Z.; Qi, S.S.; Yang, L.M.; Allen, M.B.; Niu, Y.L.; Su, L.; Li, W.F. HP–UHP meta-morphic belt in the East Kunlun Orogen: Final closure of the Proto–Tethys Ocean and formation of the PanNorth–China continent. *J. Petrol.* **2018**, *59*, 2043–2060. [CrossRef]
47. Zhang, Z.W.; Wang, Y.L.; Qian, B.; Liu, Y.G.; Dong, J. Metallogeny and tectonomagmatic setting of Ni–Cu magmatic sulfide mineralization, number I Shitoukengde mafic–ultramafic complex, East Kunlun Orogenic Belt, NW China. *Ore Geol. Rev.* **2018**, *96*, 236–246. [CrossRef]
48. Zheng, Z.; Chen, Y.J.; Deng, X.H.; Yue, S.W.; Chen, H.J. Origin of the Bashierxi monzogranite, QimanTagh, East Kunlun Orogen, NW China: A magmatic response to the evolution of the Proto–Tethys Ocean. *Lithos* **2018**, *296–299*, 181–194. [CrossRef]
49. Xin, W.; Sun, F.Y.; Li, L.; Yan, J.M.; Zhang, Y.T.; Wang, Y.C.; Shen, T.S.; Yang, Y.J. The Wulonggou metaluminous A2-type granites in the Eastern Kunlun Orogenic Belt, NW China: Rejuvenation of subduction-related felsic crust and implications for post collision extension. *Lithos* **2018**, *312–313*, 108–127. [CrossRef]
50. Wang, Y.C.; Sun, F.Y. The Middle-Late Silurian granitoids in the Eastern Kunlun Orogenic Belt, NW China: Petrogenesis and implications for tectonic evolution. *Arab. J. Geosci.* **2019**, *12*, 568. [CrossRef]
51. Tang, Y.J.; Liu, B.; Li, M.J.; Wu, Y.; Sun, Y. Origin of Devonian mafic magmatism in the East Kunlun orogenic belt, northern Tibetan Plateau: Implications for continental exhumation. *Geol. Mag.* **2020**, *157*, 1265–1280. [CrossRef]
52. Liu, Y.S.; Hu, Z.C.; Zong, K.Q.; Gao, C.G.; Gao, S.; Xu, J.; Chen, H.H. Reappraisement and refinement of zircon U-Pb isotope and trace element analyses by LA–ICP–MS. *Chin. Sci. Bull.* **2010**, *55*, 1535–1546. [CrossRef]
53. Andersen, T. Correlation of common lead in U-Pb analyses that do not report ^{204}Pb. *Chem. Geol.* **2002**, *192*, 59–79. [CrossRef]
54. Ludwig, K.R. *User's Manual for Isoplot/Ex, Version 3.00, a Geochronological Toolkit for Microsoft Excel*; Berkeley Geochronology Center Special Publication: Berkeley, CA, USA, 2003; Volume 4, pp. 1–70.
55. Li, Y.G.; Wang, S.S.; Liu, M.W.; Meng, E.; Wei, X.Y.; Zhao, H.B.; Jin, M.Q. U-Pb study of baddeleyite by LA–ICP–MS: Technique and application. *Acta Geol. Sin.* **2015**, *89*, 2400–2418. (In Chinese with English Abstract)
56. Irvine, T.N.; Baragar, W.R.A. A guide to the chemical classification of the common volcanic rocks. *Can. J. Earth Sci.* **1971**, *8*, 523–528. [CrossRef]
57. Sun, S.S.; Mcdonough, W.F. Chemical and isotopic systematics of oceanic basalts: Implications for mantle composition and processes. *Geol. Soc. Spec. Publ.* **1989**, *42*, 313–345. [CrossRef]
58. McKenzie, D.P.; Bickle, M.J. The volume and composition of melt generated by extension of the lithosphere. *J. Petrol.* **1988**, *29*, 625–679. [CrossRef]
59. Ellam, R.M. Lithospheric thickness as a control on basalt geochemistry. *Geology* **1992**, *20*, 153–156. [CrossRef]

60. Roex, A.; Dick, H.; Erlank, A.J.; Reid, A.M.; Frey, F.A.; Hart, S.R. Geochemistry, mineralogy and petrogenesis of lavas erupted along the southwest indian ridge between the bouvet triple junction and 11 degrees east. *J. Petrol.* **1983**, *24*, 267–318. [CrossRef]
61. Thompson, R.N.; Morrison, M.A.; Dickin, A.P.; Hendry, G.L. An Assessment of the relative roles of crust and mantle in magma genesis: An elemental approach. *Phil. Trans. R. Soc. Lond.* **1984**, *310*, 549–590.
62. Qian, Q.; Wang, Y. Geochemical characteristics of bimodal volcanic suites from different tectonic settings. *Geol.-Geochem.* **1999**, *27*, 29–32. (In Chinese)
63. Lassiter, J.C.; DePaolo, D.J. Plume /lithosphere interaction in the generation of continental and oceanic flood basalts: Chemical and isotopic constraints. *Am. Geophys. Union.* **1997**, *100*, 335–355.
64. Henderson, P. *Rare Earth Element Geochemistry*; Elsevier: Amsterdam, The Netherlands, 1984; Volume 2, pp. 276–280.
65. Pearce, J.A. Geochemical fingerprinting of oceanic basalts with applications to ophiolite classification and the search for Archean oceanic crust. *Lithos* **2008**, *100*, 14–48. [CrossRef]
66. Neal, C.R.; Mahoney, J.J.; Chazey, W.J. Mantle Sources and the highly variable role of continental lithosphere in basalt petrogenesis of the Kerguelen plateau and broken ridge LIP: Results from ODP Leg 183. *J. Petrol.* **2002**, *43*, 1177–1205. [CrossRef]
67. Pearce, J.A. *Trace Element Characteristics of Lavas from Destructive Plate Boundaries*; John Willey & Sons: Hoboken, NJ, USA; New York, NY, USA, 1982; pp. 525–548.
68. Wood, D.A. The application of a Th–Hf–Ta diagram to problems of tectonomagmatic classification and to establishing the nature of crustal contamination of basaltic lavas of the British Tertiary Volcanic Province. *Earth Planet. Sci. Lett.* **1980**, *50*, 11–30. [CrossRef]
69. Meschede, M. A method of discriminating between different types of mid-ocean ridge basalts and continental tholeiites with the Nb–Zr–Y diagram. *Chem. Geol.* **1986**, *56*, 207–218. [CrossRef]
70. Bian, Q.T.; Yin, L.M.; Sun, S.F.; Luo, X.Q.; Pospelov, I.; Astrakhahtsev, O.; Chamov, N. Discovery of Ordovician acritarchs in Buqingshan ophiolite complex, East Kunlun mountains and its significance. *Chin. Sci. Bull.* **2001**, *46*, 341–345. [CrossRef]
71. Wang, B.Z.; Pan, T.; Ren, H.D.; Wang, T.; Zhao, Z.Y.; Feng, J.P.; Zhang, J.M. Cambrian Qimantagh island arc in the East Kunlun orogen: Evidences from zircon U-Pb ages, lithogeochemistry and Hf isotopes of high-Mg andsite/diorite from the Lalinggaolihe area. *Earth Sci. Front.* **2021**, *28*, 318–333. (In Chinese with English Abstract)
72. Wang, B.Z.; Li, J.Q.; Fu, C.L.; Xu, H.Q.; Li, W.F. Research on formation and evolution of early Paleozoic Bulhanbuda arc in east Kunlun orogen. *Earth Sci.* **2022**, *47*, 1253–1270, (In Chinese with English Abstract).
73. Feng, J.Y.; Pei, X.Z.; Yu, S.L.; Ding, S.P.; Li, R.B.; Sun, Y.; Zhang, Y.F.; Li, Z.C.; Chen, Y.X.; Zhang, X.F.; et al. The discovery of the mafic–ultramafic melange in Kekesha area of Dulan County, East Kunlun Region, and its LA–ICP–MS zircon U-Pb age. *Geol. China* **2010**, *37*, 28–38. (In Chinese with English Abstract)
74. Cui, M.H.; Meng, F.C.; Wu, X.K. Early Ordovician island arc of Qimantag Mountain, eastern Kunlun: Evidences from geochemistry, Sm–Nd isotope and geochronology of intermediate–basic igneous rocks. *Acta Petrol. Sin.* **2011**, *27*, 3365–3379. (In Chinese with English Abstract)
75. Zhu, X.H.; Chen, D.L.; Liu, L.; Li, D. Zircon LA–ICP–MS U-Pb dating of the Wanggaxiu gabbro complex in the Dulan area, northern margin of Qaidam Basin, China and its geological significance. *Geol. Bull. China* **2010**, *29*, 227–236. (In Chinese with English Abstract)
76. Li, T.; Li, M.; Hu, C.B.; Li, Y.; Meng, J.; Gao, X.F.; Zha, X.F. Zircon U-Pb geochronology, geochemistry and its geological implications of intrusions in Aquedun area from Qimantag, East Kunlun, China. *Earth Sci.* **2018**, *43*, 4350–4363. (In Chinese with English Abstract)
77. Li, H.K.; Lu, S.N.; Xiang, Z.Q.; Zhou, H.Y.; Guo, H.; Song, B.; Zheng, J.K.; Gu, Y. SHRIMP U-Pb zircon age of the granulite from the Qingshuiquan area, central Eastern Kunlun Suture Zone. *Earth Sci. Front.* **2006**, *13*, 311–321. (In Chinese with English Abstract)
78. Zhang, J.X.; Meng, F.C.; Wang, Y.S.; Yang, J.S.; Dong, G.A. Early Paleozoic tectono-thermal event of the Jinshuikou Group on the southern margin of Qaidam: Zircon U-Pb SHRIMP age evidence. *Geol. Bull. China* **2003**, *22*, 397–404. (In Chinese with English Abstract)
79. Liu, B.; Ma, C.Q.; Guo, P.; Zhang, J.Y.; Xiong, F.H.; Huang, J.; Jiang, H.A. Discovery of the Middle Devonian A–type granite from the Eastern Kunlun Orogen and its tectonic implications. *Earth Sci.* **2013**, *38*, 947–962. (In Chinese with English Abstract)
80. Ren, J.H.; Liu, Y.Q.; Feng, Q.; Han, W.Z.; Gao, H.; Zhou, D.W. LA–ICP–MS U-Pb zircon dating and geochemical characteristics of diabase-dykes from the Qingshuiqun zrea, eastern Kunlun orogenic belt. *Acta Petrol. Sin.* **2009**, *25*, 1135–1145. (In Chinese with English Abstract)
81. Bi, H.Z.; Song, S.G.; Dong, J.L.; Yang, L.M.; Qi, S.S.; Allen, M.B. First discovery of coesite in eclogite from East Kunlun, northwest China. *Chin. Sci. Bul.* **2018**, *63*, 1536–1538. [CrossRef]
82. Bi, H.Z.; Song, S.G.; Yang, L.M.; Allen, M.B.; Qi, S.S.; Su, L. UHP metamorphism recorded by coesite-bearing metapelite in the East Kunlun Orogen (NW China). *Geol. Mag.* **2020**, *157*, 160–172. [CrossRef]
83. Zhang, Z.W.; Wang, C.Y.; Qian, B.; Li, W.Y. The geochemistry characteristics of Silurian gabbro in East Kunlun Orogenic Belt and its mineralization relationship with magmatic Ni–Cu sulfide deposit. *Acta Petrol. Sin.* **2018**, *34*, 2262–2274. (In Chinese with English Abstract)
84. Cao, S.T.; Liu, X.K.; Ma, Y.S.; Li, J.Y.; Ma, Y.L. Qimantage area Silurian intrusive rocks and its geological significance. *Qinghai Sci. Technol.* **2011**, *18*, 26–30. (In Chinese with English Abstract)

85. Liu, B.; Ma, C.Q.; Jiang, H.A.; Guo, P.; Zhang, J.Y.; Xiong, F.H. Early Paleozoic tectonic transition from ocean subduction to collisional orogeny in the eastern Kunlun Region: Evidence from Huxiaoqin mafic rocks. *Acta Petrol. Sin.* **2013**, *29*, 2093–2106. (In Chinese with English Abstract)
86. Gao, Y.B.; Li, W.Y.; Qian, B.; Li, K.; Li, D.S.; He, S.Y.; Zhang, Z.W.; Zhang, J.W. Geochronology, geochemistry and Hf isotopic compositions of the granitic rocks related with iron mineralization in Yemaquan deposit, East Kunlun, NW China. *Acta Petrol. Sin.* **2014**, *30*, 1647–1665. (In Chinese with English Abstract)
87. Han, Z.H.; Sun, F.Y.; Tian, N.; Gao, H.C.; Li, L.; Zhao, T.F. Zircon UPb geochronology, geochemistry and geological implications of the Early Paleozoic Wulanwuzhuer granites in the Qimantag, East Kunlun, China. *Earth Sci.* **2021**, *46*, 13–30. (In Chinese with English Abstract)
88. Wang, G.; Sun, F.Y.; Li, B.L.; Li, S.J.; Zhao, J.W.; Ao, C.; Yang, Q.A. Petrography, zircon U-Pb geochronology and geochemistry of the mafic-ultramafic intrusion in Xiarihamu Cu–Ni deposit from East Kunlun, with implications for geodynamic setting. *Earth Sci. Front.* **2014**, *21*, 381–401. (In Chinese with English Abstract) [CrossRef]
89. Wang, Y.L.; Li, Y.J.; Wei, J.H.; Li, H.; Han, Y.; Zhou, H.Z.; Huang, X.K.; Ke, K.J. Origin of Late Silurian A–type granite in Wulonggou area, East Kunlun Orogen: Zircon U-Pb age, geochemistry, Nd and Hf isotopic constraints. *Earth Sci.* **2018**, *43*, 1219–1236. (In Chinese with English Abstract)
90. Liu, B.; Wu, L.H.; Ma, C.Q.; Xu, Y.; Li, F.L.; Zhang, J.M.; Huang, J.; Sun, Y. Petrogenesis and Tectonic Implications of Silurian to Devonian Intermediate Rocks from the East Part of the Eastern Kunlun Orogenic Belt. Available online: https://kns.cnki.net/kcms/detail/42.1874.P.20220530.2100.018.html (accessed on 25 December 2022). (In Chinese with English Abstract)
91. Wang, P.X.; Guo, F.; Wang, Z.N. Zircon U-Pb geochronology, geochemistry and geological significance of granitoids in the Yazigou, Qimantage Area of East Kunlun Mountains. *Geosci* **2020**, *34*, 987–1000. (In Chinese with English Abstract)
92. Wang, P.X.; Guo, F.; Wang, Z.N.; Feng, N.Q. Zircon U-Pb ages, geochemical features and constraints on regional tectonic evolution of gabbro–diabase in Xiaoyuanshan area, Qimantage of East Kunlun Mountains. *Geol. Bull. China* **2022**, *41*, 1169–1183. (In Chinese with English Abstract)
93. Zhang, L.; Li, B.L.; Liu, L.; Wang, P.X.; Li, L. Geochronology, geochemistry and geological significance of the Early Devonian bimodal intrusive rocks in Wulonggou area, East Kunlun Orogen. *Acta Petrol. Sin.* **2021**, *37*, 2007–2028. (In Chinese with English Abstract)
94. Liu, B.; Ma, C.Q.; Zhang, J.Y.; Xiong, F.H.; Huang, J.; Jiang, H.A. Petrogenesis of Early Devonian intrusive rocks in the east part of Eastern Kunlun Orogen and implication for Early Palaeozoic orogenic processes. *Acta Petrol. Sin.* **2012**, *28*, 1785–1807. (In Chinese with English Abstract)
95. Hao, N.N.; Yuan, W.M.; Zhang, A.K.; Cao, J.H.; Chen, X.N.; Feng, Y.L.; Li, X. Late Silurian to Early Devonian granitoids in the Qimantage area, East Kunlun Mountains: LA–ICP–MS zircon U-Pb ages, geochemical features and geological setting. *Geol. Rev.* **2014**, *60*, 201–215. (In Chinese with English Abstract)
96. Lu, L.; Wu, Z.H.; Hu, D.G.; Barosh, P.J.; Hao, S.; Zhou, C.J. Zricon U-Pb age for rhyolite of the Maoniushan Formation and its tectonic significance in the East Kunlun Mountains. *Acta Petrol. Sin.* **2010**, *26*, 1150–1158. (In Chinese with English Abstract)
97. Davies, J.H.; Von Blanckenburg, F. Slab breakoff: A model of Lithosphere Detachment and its test in the magmatism and deformation of collisional orogens. *Earth Planet. Sci. Lett.* **1995**, *129*, 85–102. [CrossRef]
98. Bonin, B. Do Coeval mafic and felsic magmas in post–collisional to withinplate regimes necessarily imply two contrasting, mantle and crustal, sources? A review—ScienceDirect. *Lithos* **2004**, *7*, 1–24. [CrossRef]
99. Dokuz, A. A slab detachment and delamination model for the generation of Carboniferous high–potassium I–type magmatism in the Eastern Pontides, NE Turkey: The Köse composite pluton. *Gondwana Res.* **2011**, *19*, 926–944. [CrossRef]